RSC Advances

PAPER

View Article Online
View Journal | View Issue

Cite this: *RSC Adv.*, 2014, **4**, 29383

Control of active semiconducting layer packing in organic thin film transistors through synthetic tailoring of dielectric materials†

Ranjodh Singh,[a] Jagan Singh Meena,*[ab] Yu-Cheng Chang,[a] Chung-Shu Wu[a] and Fu-Hsiang Ko*[a]

Received 10th March 2014
Accepted 19th June 2014

DOI: 10.1039/c4ra02077d

www.rsc.org/advances

Apart from the development of new dielectric and semiconductor materials, the semiconductor–dielectric interface study is also very important for the optimum performance of organic thin film transistors (OTFTs). Herein, we have reported the detailed synthesis of a whole new family of dielectric materials which are 1,3,5,7-tetrabromoadamantane; 1,3,5,7-tetrachloroadamanatane; 1,3,5,7-tetraiodoadamantane and 1,3,5,7-tetrauraciladamantane ($AdUr_4$). The unique ability of these molecules to undergo supramolecular thin film formation at low temperature, was analysed for their potential use as an insulator in organic electronic devices. Owing to the good leakage current density property shown by $AdUr_4$ dielectric material it was further employed as a gate dielectric in regioregular poly(3-hexylthiophene), (P3HT) based OTFT. This OTFT device which was fabricated on a flexible PI plastic substrate has shown a good on/off current ratio (*e.g.*, 2.18 × 10^4) and high mobility (*e.g.*, 0.15 $cm^2\ V^{-1}\ s^{-1}$). The semiconductor–dielectric interface study, has revealed that the $AdUr_4$ gate dielectric layer has guided the P3HT molecular chain domains to undergo edge-on orientation, which is the charge transport direction in OTFTs. In this process, the grazing incidence X-ray diffraction (GI-XRD) analysis and AFM study was also employed.

1. Introduction

Organic thin film transistors (OTFTs) have been emerging as a new class of organic electronic devices, with a potential to replace the traditional silicon based transistors.[1] They are expected to play a major role in future for the development of low cost electronic devices which will be tough, light weight and flexible.[2] They have been the focus of research for the development of flexible electronics because of their cost-effective production, solution based processability and compatibility with variety of flexible substrates.[3] Instead of so much merits associated with them, there are lot of challenges needs to be met before their commercialization for practical uses such as in the field of displays, sensors, invertors and radio frequency identification tags.[4] The major hurdle coming in the commercialization of OTFTs is mainly due to their low output current and high operating voltage, as resulting from low charge carrier mobility of the active semiconducting layer employed respectively in them.[5] In general, OTFTs are composed of three components namely an electrode, semiconducting layer and a dielectric insulating layer separating the active semiconducting material from a gate electrode. Thus the performance of OTFTs can be improved either by employing an organic semiconducting with better charge carrier mobility or with the use of dielectric material having low leakage current and high dielectric constant.[6] In past various research groups have successfully achieved the high charge carrier mobility, $\mu_{FE} \approx 10\ cm^2\ V^{-1}\ s^{-1}$ by employing new organic semiconductor materials in OTFTs.[7] However, the dielectric layer which also plays an important role in working of OTFTs, has been less explored as compared to semiconductor materials.[8] The mobility and threshold voltage of OTFTs in the linear regime are related by the equation,[9]

$$I_{DS} = \frac{WC_i}{L}\mu_{FE}\,(V_G - V_{th})V_{DS} \quad (1)$$

where, I_{DS} and V_{DS} are the current and voltage bias between source and drain, respectively, V_G denotes the gate voltage at which the current starts to rise. Further, W and L denotes the source–drain width and length, respectively; μ_{FE} is the field effect mobility; C_i is the capacitance per unit area of the insulator, and V_{th} is the threshold voltage. Thus, the proper choice of the dielectric material having low leakage current and high capacitance is essential for the low operating voltage OTFTs.[10] The field induced charge carriers are confined to the thin region *i.e.* interface between semiconductor and dielectric layer in OTFTs.[11] Hence, in combination with the development of new

[a]*Department of Materials Science and Engineering, National Chiao Tung University, Hsinchu, Taiwan. E-mail: fhko@mail.nctu.edu.tw; jaganphy@gmail.com; Fax: +886-35744689; Tel: +886-35712121 ext. 55803*

[b]*Department of Electronics Engineering, National Chiao Tung University, Hsinchu, Taiwan*

† Electronic supplementary information (ESI) available. See DOI: 10.1039/c4ra02077d

dielectric and semiconductor materials, the semiconductor–dielectric interface study is also pivotal for the optimum performance of OTFTs.[12] Kim *et al.* have also reported,[12a] the effect of dielectric surface modification on the field-effect mobility of regioregular poly(3-hexylthiophene) (P3HT) based transistor. When the silicon dioxide SiO_2 insulator substrate was modified with –OH terminated self-assembled monolayers (SAM), μ_{FE} was 0.08 $cm^2\ V^{-1}\ s^{-1}$. However, upon SiO_2 surface modification with $-NH_2$ terminated SAM, the mobility increased by several orders of magnitude of 0.28 $cm^2\ V^{-1}\ s^{-1}$ for the same P3HT semiconductor. This was due to the difference in orientation (perpendicular and parallel) of P3HT chains with respect to the modified SiO_2 insulator substrate which lead to the difference in behaviour of device performance. Recently, Jenn-Chang Hwang *et al.* have reported[13] the use of silk fibroin as a dielectric on the flexible poly(ethylene terephthalate) (PET) plastic substrate for the fabrication of pentacene OTFTs. The planner structure of the silk fibroin dielectric has allowed the pentacene molecules to self-assemble in the planner form which resulted in a very high μ_{FE} value of 23.2 $cm^2\ V^{-1}\ s^{-1}$ in the saturation regime and a low operating voltage of −3 V. Hence, the proper choice of dielectric material with a good compatibility with the active semiconducting layer is also essential for the optimum performance of OTFTs.

Organic and polymeric materials have been extensively explored in recent years for their potential use as a gate dielectric in OTFTs. Nowadays, they are widely pursued over traditional SiO_2 dielectric because of their low cost and their ability to form high quality thin films from them can be prepared by simple processing methods. These are spin coating, ink-jet printing and sol–gel process.[14] Some of the most extensively explored polymers in this field are poly(methyl methacrylate) (PMMA), poly(styrene) (PS), poly(4-vinyl phenol) (PVP), poly(acrylic acid) (PAA), and poly(perfluorobutenyl vinyl ether) (CYTOP).[15] These polymer gate dielectrics are known to have low leakage current which leads to the performance enhancement of OTFTs. However, due to their solubility in common organic solvents these polymer dielectrics get washed away during the deposition of organic semiconducting material by dip coating or spin coating methods.[16] Some research groups have achieved the dielectric thin film of thickness <50 nm with high breakdown voltages by thermally crosslinking of the gate dielectric material.[17] However, the curing temperature as needed for this process is higher than the glass transition temperature of flexible substrate.[18] This leads to the poor performance of device. Therefore, there is a strong desire to design new organic dielectric materials which should be processable into thin film at low temperature from their solution in specific solvents.

Diamond is also a good insulator material,[19] however its high cost, restricts its use as a gate dielectric in low cost OTFTs. On the other hand, the adamantane, (chemical formula $C_{(4n+6)}H_{(4n+12)}$, where $n = 0, 1, 2, 3\ldots$), which is the smallest cage structure of diamond, is cheap and can be easily obtained from oil and natural gas condensates after purification.[20] This structurally rigid, thermally stable (pyrolysis temperature >660 °C) and easy to be chemically modified[21] diamondoid molecule has recently been reviewed by Schwertfeger *et al.*[22] The spatial arrangement of carbon atoms in adamantane is similar to that in diamond lattice.[23] It has been broadly studied for its numerous applications in biology and chemistry.[24]

Motivated by so much merits associated with adamantane, we modified adamantane surface structure, chemically to synthesize its four derivatives namely; 1,3,5,7-tetrabromoadamantane ($AdBr_4$); 1,3,5,7-tetrachloroadamanatane ($AdCl_4$); 1,3,5,7-tetraiodoadamantane (AdI_4) and 1,3,5,7-tetrauraciladamantane ($AdUr_4$). The solution of these functionalized molecules has the ability to undergo smooth thin film formation at low temperature through supramolecular self-assembly (STF) (Scheme 1). The halogen–halogen interactions, van der Waals force of attractions and electrostatic force of attractions have played an important role in supramolecular polymeric thin films formation of $AdBr_4$, $AdCl_4$, AdI_4. This unique ability of these small nanodiamond molecules to undergo thin film formation, with network structure similar to that of diamond lattice has prompted our group to explore their potential application as an insulator in organic electronics. This was analysed by employing these materials as insulating layer in MIM devices, as fabricated on flexible polyimide (PI) plastic substrate. The scanning electron microscope (SEM) study was employed to study morphology of organic dielectric thin films and further its effect was explored on MIM device performances as based on them. The difference in morphology of $AdBr_4$, $AdCl_4$, AdI_4 STF has prevailed because of the different type of intermolecular forces involved in their formation. This was determinant in MIM device performance based on them. To further explore the effect of intermolecular forces on dielectric STF and its subsequent effect on the electrical performance of device we synthesised another unique derivative of adamantane, *i.e.* $AdUr_4$. The uracil substituents on the surface of $AdUr_4$ molecules has allowed them to adsorb on the gold coated

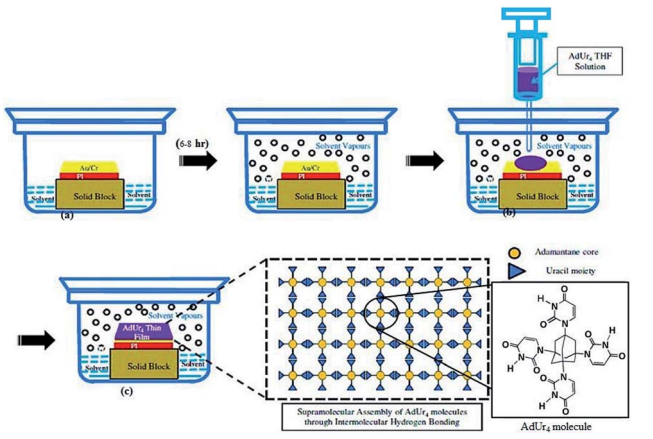

Scheme 1 Schematic representation of the $AdUr_4$ insulator supramolecular thin film formation on flexible PI plastic substrate: (a) flexible PI coated with Au/Cr layer is placed on a rigid support (solid block) in a beaker containing the solvent (THF) (b) injecting the drops of $AdUr_4$ solution on this PI plastic substrate after 3–4 hours (c) the small rigid $AdUr_4$ molecules self-assemble through U···U intermolecular hydrogen bonding into the form of a thin film. This last process takes 5–6 hours.

flexible PI plastic substrate. Moreover, with Fourier transform infrared (FTIR) spectroscopy, it has been found that these $AdUr_4$ molecules have undergone lateral interaction with each other through uracil–uracil (U···U) intermolecular hydrogen bonding that has led to the formation of their STF. Because of this the MIM devices as fabricated from $AdUr_4$ STF showed better insulator properties as compared to that of $AdBr_4$, $AdCl_4$, AdI_4 STF. The thermal stability of $AdUr_4$ STF based MIM devices, was further analysed by heating them to various temperature and then measuring the leakage current at that corresponding temperature. The variable temperature FTIR spectroscopy was performed to find out the effect of heat on intermolecular hydrogen bonding involved in $AdUr_4$ dielectric thin film. After this detailed analysis study of $AdUr_4$ dielectric thin film, we employed it as a gate dielectric material in the P3HT based OTFTs with bottom gate and top contact. Through semiconductor–dielectric interface study, it has been found, that the unique rigid structure of $AdUr_4$ has guided the regioregular P3HT chain domains to crystallize in edge-on orientation. The GI-XRD and atomic force microscopy study (AFM) was performed to successfully explore this phenomenon. The edge-on conformation has increased the charge carrier transfer to in-plane direction of P3HT chains which has led to the success of $AdUr_4$ as a gate dielectric in P3HT based OTFTs with good on/off current ratio.

2. Experimental section

2.1 Reagents and materials

1-Bromoadamantane (99%), bromine (99.5%) and iodomethane was procured from Sigma Aldrich and used as received. Aluminum chloride and aluminum bromide anhydrous, powder of 99.999% trace metal basis was supplied by Alfa Aesar. The dichloromethane, chloroform and tetrahydrofuran (THF) obtained from Alfa Aesar were dried and distilled from sodium/benzophenone prior to their use. Chromium shots (Cr, 99.999%, Admat Inc.) 3–5 mm in size, aluminium shots (Al, 99.999%, Admat Inc.) 3–5 mm in size, and gold shots (Au, 99.999%, Admat Inc.) 1–2 mm in size, were purchased from Gredmann Taiwan Ltd. The organic semiconductor regioregular poly(3-hexylthiophene) (P3HT catalog number 698997 electronic grade, purchased from Aldrich, average molecular weight M_n 54 000–75 000, >98% head-to-tail regioregular) was adopted for this research. DuPont Kapton Polyimide film, 38 μm in thickness and from PV9100 series was used as substrate to fabricate the device.[25] All other reagents and solvents were obtained from commercial suppliers and used as such, unless specified. It should be noted that all experiments were performed under dry nitrogen atmosphere and in standard fume hood.

2.2 Dielectric thin film preparation and fabrication of the MIM and OTFT devices

Scheme 1 presents the general method[26] for the preparation of the respective dielectric thin films of $AdBr_4$, $AdCl_4$, AdI_4, and $AdUr_4$. In a typical thin film preparation experiment $AdUr_4$ (0.05 mg) was dissolved in (10 mL) of THF under static conditions at 50 °C for 30 minutes. It was filtered with micro-syringe before drop casting on PI substrate. The dielectric thin film from tetrahedral molecules of adamantane derivatives were produced by their slowly self-assembling from a solution (0.05 mg mL^{-1}) under a certain solvent pressure in a closed jar, as depicted in Scheme 1. It should be noted, that the solvent in the bottom of the jar was very crucial for the formation of well-defined smooth thin film from adamantane derivatives, which could play two important roles: (1) slow evaporation of the solvent guaranteed the small tetrahedral molecules had sufficient time to adjust themselves and come closer together with strong intermolecular interactions so that they can further self-assemble into smooth thin film on the substrate; (2) certain solvent vapour pressure in the upper space of the jar could guarantee the free movement of these molecules and then induced them to assemble together leading to the growth of polymer like film on the substrate. Apart from $AdUr_4$ which have good solubility in THF the other halogen derivatives of adamantane as reported here, have good solubility in all organic solvents such as toluene, chloroform, chlorobenzene. However, the good solubility of all adamantane derivatives in THF and low vapor pressure of THF has prompted us to finally choose THF as a solvent of choice for the respective STF preparation of all the adamantane derivatives in this work.

A DuPont Kapton plastic PI plastic substrate with a thickness of 38 μm was used as the flexible substrate for the fabrication of MIM capacitor and OTFT devices. The PI plastic substrate was ultrasonically cleaned using ethanol (Fluka; water content: <0.1%) for 30 min and then rinsed with DI water. A high-pressure stream of N_2 gas was then used to remove the water and any remaining particles from the PI surface. After being cleaned, the PI plastic substrate was annealed at 200 °C for 1 h under vacuum to achieve relative thermal stability and to enhance the adhesion strength. Next, Cr (20 nm thick) and Au (80 nm thick) were sequentially deposited onto the PI plastic substrate using a thermal coater. The Cr layer was used as the adhesion layer between the PI plastic substrate and the Au thin film.[27] Au was deposited as a gate electrode over the Cr layer on the PI plastic substrate. This PI was then placed in a jar containing the THF solvent and the jar was covered for 6–8 h to maintain a suitable vapour pressure inside it as shown in Scheme 1. Finally, the filtered THF solution of $AdUr_4$ was drop casted over this PI plastic substrate using a syringe in such a way that it should cover the whole PI surface. After, the complete evaporation of solvent from the PI plastic substrate as evaporated; it was heated at 40 °C for 10 min to remove any solvent trapped inside the dielectric film, formed by self-assembly of molecules. At the end of this experiment, Al films with a thickness of 300 nm were patterned as the top electrode using a shadow mask and a thermal coater.

The electrical insulating properties of the halogen and uracil adamantane derivatives respective thin films have been optimized for OTFT on the PI plastic substrate. For OTFT device fabrication Cr and Au, which had thickness of 20 and 80 nm, respectively, were sequentially deposited through a shadow mask using a thermal coater to function as gate electrodes.

Then, gate dielectric $AdUr_4$ thin film was prepared on it, as described in Scheme 1. The P3HT film was then deposited as a channel layer using a spin casting method, at room temperature and annealed at 40 °C for 30 minutes. Finally, source (S) and drain (D) Al electrodes with a thickness of 100 nm were deposited onto the Al/P3HT/$AdUr_4$/Au/Cr/PI through a shadow mask, which yielded the top-contact electrode OTFTs. The channel length (L) and width (W) were 82 μm and 2000 μm, respectively.

2.3 Thin film characterizations and electrical measurements

The surface morphology of the $AdBr_4$, $AdCl_4$, AdI_4 and $AdUr_4$ respective self-assembled thin films on the PI plastic substrate was evaluated using scanning electron microscope (SEM, JEOL). The thicknesses of these films were estimated by optical ellipsometry techniques. The surface morphology of the P3HT film that was spin casted over insulator substrate on the PI plastic substrate was evaluated using atomic force microscopy (AFM, Digital Instruments Nanoscope, D-5000) with a scan size of 2 μm × 2 μm and a scan rate of 1 Hz. The FTIR spectrum was recorded using the FTIR spectrometer (model 580, Perkin-Elmer) with a resolution of 4.00 cm^{-1}. An infrared spectrum was recorded under nitrogen atmosphere in the range of 500–4000 cm^{-1} to determine the functional groups in the molecular structure. The samples were prepared on PI substrate (1 × 1 cm^2) for FTIR measurement. Further, variable temperature FTIR experiments were performed on $AdUr_4$ STF. The $AdUr_4$ thin film was prepared on PI plastic substrate (1 × 1 cm^2) by following the procedure as shown in Scheme 1. This PI plastic substrate was then *in situ* heated from 40–120 °C under nitrogen flow (20 mL min^{-1}) in a FTIR instrument equipped with temperature controller function. Corresponding to each temperature, FTIR spectrums were recorded for this $AdUr_4$ STF. The XRD pattern for the organic P3HT film was recorded using a Rigaku D/max-IIIB diffractometer with Cu Kα radiation (λ = 1.5406 Å). The sample for XRD study was prepared by spin casting the THF solution of P3HT on the $AdUr_4$ dielectric STF with PI as the substrate.

MIM Capacitor. To investigate, the electrical characterization of all the four adamantane derivatives dielectric thin films, the capacitance–voltage (C–V) and the leakage current–voltage (I–V) were measured using a HP-4284A C–V analyser and Agilent-4156 probe station, respectively. The real part of the dielectric constant (k) was calculated using the following formula

$$k = \frac{Ct}{\varepsilon_o A_m} \quad (2)$$

in which C is capacitance, t is the thickness of the dielectric film (measured by ellipsometry technique), A_m the capacitance area, and ε_o the permittivity of vacuum. The leakage current was measured in direct current on the capacitors in the range 0–100 V with a holding time of 100 ms (Agilent 4156). A quasi-static capacitance *versus* voltage curve was taken at a sweep rate of 0.25 V s^{-1} using a Keithley 595 quasi-static C–V meter. We examined an additional property for $AdUr_4$ dielectric based MIM device, to check its stability against the temperature. This was done by heating the MIM device to various temperatures and measuring the leakage current at that respective temperature.

OTFT device. The electrical characteristics of the transistors were measured in a nitrogen glove box on an Agilent-4156 probe station. The transistor parameters, such as charge carrier mobility, were calculated using the standard formalism of field-effect transistors in the linear and saturation regimes respectively. The P3HT based OTFTs exhibits output characteristics with pinch off and current saturation. The electrical characteristics of the P3HT based OTFTs are very stable during operation. The μ_{FE} value in the linear region (μ_{FE}, lin) is obtained from the transfer characteristics using eqn (1). The C_i value for the P3HT thin film transistor was measured using MIM structure fabricated next to the P3HT based OTFT device.

3. Results and discussion

The adamantane, a tricyclic saturated hydrocarbon (tricyclo [3.3.1.1]decane) is the smallest "nanodiamond" molecule.[26] Its bulky molecular volume, rigidity and highly symmetrical tetrahedral shape makes it an ideal building block for nanofabrication.[21,24] Our research group have took the advantage of this unique rigid structure of adamantane for its application, as an insulator in flexible organic electronic devices, first in MIM devices and then finally in OTFTs. The ability of adamantane molecule to undergo substitution reaction readily at its 1,3,5,7 position allowed us to prepare its four derivatives.[20e] These are $AdBr_4$, $AdCl_4$, AdI_4, $AdUr_4$, and was synthesized by following the Scheme 2. The STF of these compounds were prepared on flexible PI plastic substrate, as illustrated in Scheme 1 for their application as an insulator in MIM and OTFTs devices. It has been found that the supramolecular interactions, has guided these individual small rigid molecules to self-assemble[28] in form of their rigid and flexible thin films. The STF of $AdBr_4$, $AdCl_4$, AdI_4 molecules have occurred through halogen–halogen interactions *i.e.* Br···Br, Cl···Cl, I···I respectively.[29–31] However, the $AdUr_4$ molecules have knitted up together in the form of STF through U···U intermolecular hydrogen bonding.[32] The Fig. 1

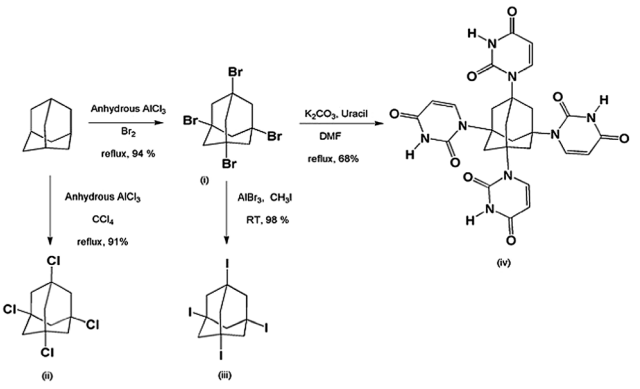

Scheme 2 Synthetic route[27] of dielectric materials based on adamantane ($AdBr_4$, $AdCl_4$, AdI_4, $AdUr_4$).

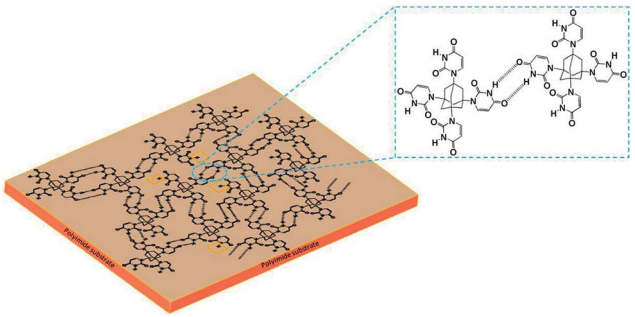

Fig. 1 U···U intermolecular hydrogen bonding in $AdUr_4$ molecules leading to their STF formation on the flexible PI plastic substrate. Free –NH (not involved in U···U intermolecular hydrogen bonding) are shown in yellow square box.

shows that in $AdUr_4$ STF each $AdUr_4$ molecule is involved in intermolecular hydrogen bonding with nearby $AdUr_4$ molecules.

Furthermore, through FTIR study we also confirmed the presence of some free –NH (not involved in U···U intermolecular hydrogen bonding) of uracil in $AdUr_4$ STF.

The difference in the respective STF of $AdBr_4$, $AdCl_4$, AdI_4, $AdUr_4$ is because of the different type of intermolecular forces involved in their formation. Due to this they have exhibited the different leakage current density, when employed as an insulating layer, in MIM devices. The *I–V* characteristics of these respective MIM devices are shown in ESI (Fig. S5–S8†). In Fig. 2, we have compared the leakage current density (capacitor area = 0.01 mm^2) of these MIM devices and corresponding results has been shown in Table 1. The leakage current density of $AdUr_4$, MIM device is 2.28×10^{-9} A cm^{-2} while the leakage current density of MIM devices based on $AdCl_4$, $AdBr_4$, AdI_4 insulating materials are 1.74×10^{-6} A cm^{-2}, 2.74×10^{-7} A cm^{-2} and 6.01×10^{-8} A cm^{-2} respectively. From this it can be concluded that the $AdUr_4$ STF is an excellent insulator material followed by that of AdI_4, $AdBr_4$, and $AdCl_4$. The good leakage current density of $AdUr_4$ STF has motivated us to carry our further study to explore its potential use as a gate dielectric in OTFTs. Moreover, we have also measured the capacitance for these films and found the low dielectric constants, which are 2.1 for $AdCl_4$, 2.09 for $AdBr_4$ and 2.4 for AdI_4. But, the better capacitance (209.0 nF cm^{-2}) was measured for $AdUr_4$ STF with better dielectric constant (2.6) than the other three films. Moreover, the thicknesses of $AdCl_4$, $AdBr_4$, AdI_4 and $AdUr_4$ films as estimated by ellipsometry are 10.2, 10.7, 11.5 and 11.0 nm respectively.

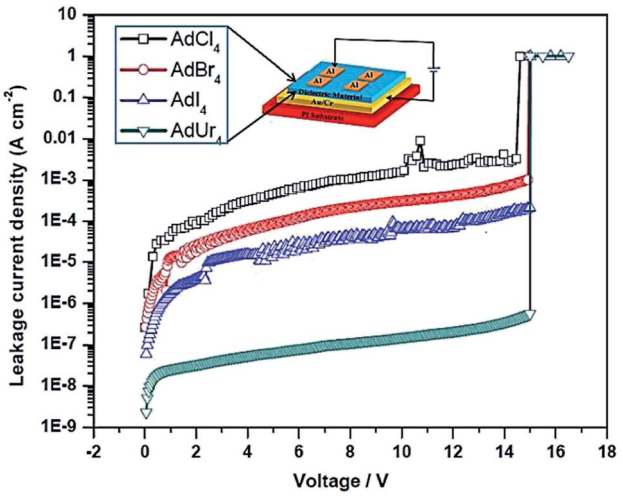

Fig. 2 Comparison of leakage current behaviour of $AdCl_4$, $AdBr_4$, AdI_4 and $AdUr_4$.

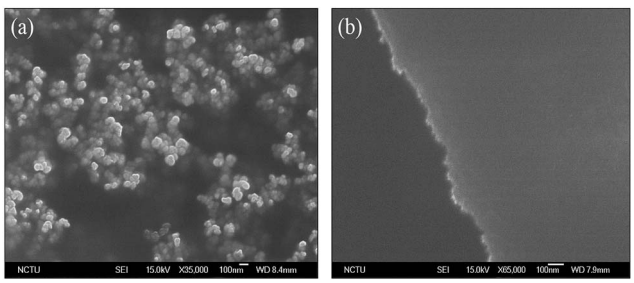

Fig. 3 SEM image of (a) $AdUr_4$ STF when prepared from THF solution of $AdUr_4$ without following Scheme 1, (b) supramolecular thin film formed from THF solution of $AdUr_4$ by following the Scheme 1.

It has been found that the difference in morphology of STF formed by these respective materials on PI plastic substrate has led to this difference in their electrical performance of MIM devices based on them.[33] The $AdBr_4$, $AdCl_4$, AdI_4 are well known to form plastic crystals through X···X interactions, as do other symmetrical adamantane derivatives. Pedireddi *et al.*, have also reported[30] that X···X (where X = Cl, Br, I) interactions can be represented as specific attractive forces. The attractive nature of X···X contacts depend on atomic polarization of respective halogen atoms, which varies as follow.[34]

$$Cl\cdots Cl < Br\cdots Br < I\cdots I$$

The atomic size of chlorine, bromine and iodine atoms are 0.99 Å, 1.15 Å and 1.40 Å respectively.[35] The I···I attractive

Table 1 Summary of all the characteristic properties of $AdCl_4$, $AdBr_4$, AdI_4 and $AdUr_4$ when incorporated as insulator layer in MIM devices

Dielectric material	Thickness (nm)	Dielectric constant	Capacitance density (nF cm^{-2})	Leakage current density (A cm^{-2})
$AdCl_4$	10.2	2.1	182.0	1.74×10^{-6}
$AdBr_4$	10.7	2.09	172.0	2.74×10^{-7}
AdI_4	11.5	2.4	185.4	6.01×10^{-8}
$AdUr_4$	11.0	2.6	209.0	2.28×10^{-9}

contacts appeared because of electron cloud distortion of iodine atoms further leading to the formation of partial positive and negative charge on them. Thus, the I···I contacts that have prevailed in AdI_4 STF are because of electrostatic forces of attractions among iodine atoms.[30] Owing, to the larger atomic size, this distortion of electron clouds is much more pronounced in case of iodine atoms as compared to that of bromine and chlorine atoms. The X···X (where X = Cl, Br) that are present respectively in $AdCl_4$, $AdBr_4$ STF are because of van der Waals (vdW) interactions (attractive). Each molecule of $AdBr_4$ has been interacted with the nearby two or three molecules of $AdBr_4$ through these Br···Br vdW interactions.[36] The vdW interactions are known to be of weaker strength as compared to that of electrostatic forces of attractions and intermolecular hydrogen bondings.[37] Hence, due to weak intermolecular forces, $AdBr_4$ molecules in its STF are not packed as closely as that of AdI_4 molecules in AdI_4 STF. Further, the smaller atomic size of chlorine atoms has resulted into more weaker X···X (X = Cl) vdW interactions among $AdCl_4$ molecules resulting into the more loose packing of the $AdCl_4$ molecules in their STF.[31,34] The effect of this intermolecular interactions on molecular packing on surface morphology of STF was further analysed by SEM. It has been found that the AdI_4 STF has smaller cracks followed by that of $AdBr_4$ and $AdCl_4$ (SEM images of these STF are shown in ESI S1–S3†). Due to this difference in surface quality of AdX_4 (X = Cl, Br, I) STF, the MIM devices based on them has showed the difference in their electrical performance.[38] The halogen–halogen interactions are the weaker intermolecular forces of interactions as compared to that of intermolecular hydrogen bonds.[39] Therefore, when $AdUr_4$ STF were analysed by SEM, they appeared to be smooth with no pinholes or cracks, as shown in Fig. 3b. The SEM image in Fig. 3a shows the $AdUr_4$ STF when prepared from its low concentration solution on PI plastic substrate (without following Scheme 1) appeared as cluster of $AdUr_4$ molecules. In this case, the THF solution of $AdUr_4$ was drop casted on PI plastic substrate and allowed to dry it in open atmosphere.

We found that, for preparation of $AdUr_4$ STF on PI plastic substrate by Scheme 1, has played a significant role in the formation of its smooth STF. In this method, the slow evaporation of solvent gives sufficient time to $AdUr_4$ molecules to move closer to each other and then self-assemble in the form of their STF through U···U intermolecular hydrogen bonds.[32] The $AdUr_4$ molecules undergoes adsorption on gold coated surface layer (bottom electrode for MIM and OTFTs devices) on PI plastic substrate through uracil groups. This adsorption holds the individual $AdUr_4$ molecules strongly against the gold coated PI plastic substrate.[40] These molecules further interacts laterally with each other through intermolecular hydrogen bonding between uracil groups as shown in Fig. 1. In this process, –NH and –CO present in imide functional group of uracil acts as the donor and acceptor respectively, leading to the formation of rigid STF of $AdUr_4$ on gold coated PI plastic substrate.

The role played by U···U intermolecular hydrogen bonds on stability of the $AdUr_4$ STF was further characterized by variable temperature FTIR spectrometer.[41] The $AdUr_4$ STF on PI plastic substrate was heated to various temperatures and

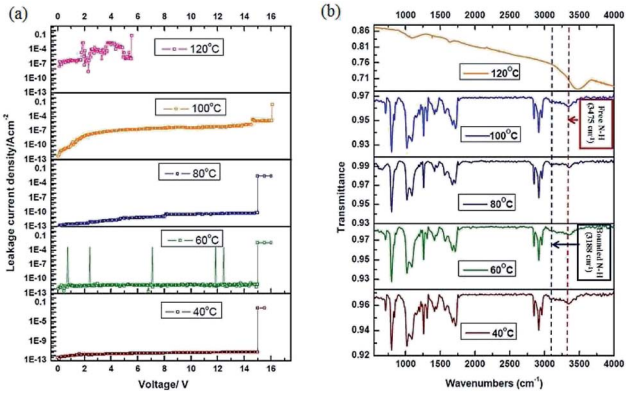

Fig. 4 (a) *I–V* characteristic property under different temperature of flexible 5 × 5 cm^2 MIM device incorporated with $AdUr_4$ insulator layer (b) corresponding variable temperature FTIR spectra of the $AdUr_4$ STF as prepared on flexible PI plastic substrate.

corresponding to each temperature the leakage current property of MIM capacitor device was analysed as shown in Fig. 4.

It has been found that MIM devices, incorporated with $AdUr_4$ STF as an insulator has shown good electrical performance up to 100 °C. This can be seen in terms of its high leakage current density, 3.30×10^{-3} A cm^{-2} at 120 °C as calculated from its *I–V* characteristics curve in Fig. 4a. This has been attributed to breakage of U···U intermolecular hydrogen bonds at 120 °C, which has prevailed in $AdUr_4$ STF. The variation in FT-IR spectra of $AdUr_4$ thin film at 120 °C, in Fig. 4b shows this change. Hence, the excellent electrical performance shown by MIM devices incorporated with $AdUr_4$ STF is due to the U···U intermolecular hydrogen bonds in them. The FTIR spectra of $AdUr_4$ STF in Fig. 4b, shows the characteristic peaks corresponding to those of the free amide NH groups at 3475 cm^{-1} and that of –NH involved in U···U interactions at 3188 cm^{-1}.[41c] Thus, the U···U intermolecular hydrogen bonds has played a significant role in success of the $AdUr_4$ STF as new dielectric layer in flexible MIM device at high temperature. The success of $AdUr_4$ STF based MIM devices, have prompted us to incorporate it as a gate dielectric layer in OTFTs.

In order to study the potential of the $AdUr_4$ STF as a dielectric layer, we fabricated a P3HT based OTFTs with a bottom gate and top contact having a channel width of 2000 μm and a channel length of 82 μm (Fig. 5a). The Fig. 5b shows the photographic optical image of OTFTs as fabricated on flexible PI plastic substrate with its corresponding configuration shown in Fig. 5a. The Fig. 5c, shows the transfer characteristics for OTFTs. The Fig. 5d, presents the drain current–drain voltage (I_{DS}–V_{DS}) output curve as obtained from our OTFT with a 11.0 nm thick $AdUr_4$ dielectric layer, which is prepared according to Scheme 1. The device demonstrated, desirable OTFT characteristics at an operating voltage lower than −45 V. Maximum saturation current of 0.26 μA was achieved. The observed OTFT characteristics confirmed closely to conventional transistor models in both the linear and saturation regimes with I_{DS} increasing linearly at low drainage voltage, and clear saturation behaviour at high drain voltage. According to the drain current–gate

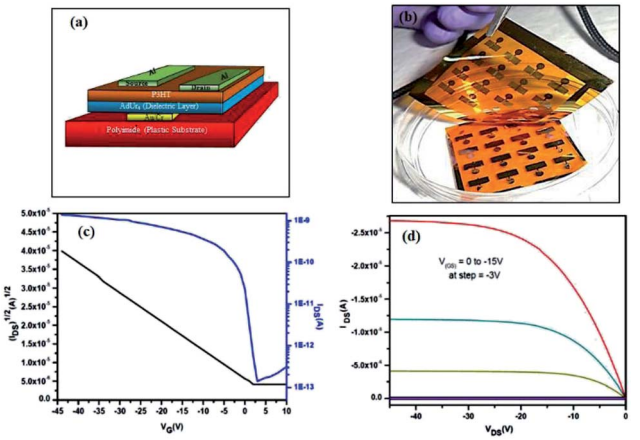

Fig. 5 (a) Schematic diagram of bottom gate OTFT device that features $AdUr_4$ as a gate insulator and P3HT as a semiconducting layer (b) photograph of the OTFT devices on a 5 × 5 cm^2 area on a flexible PI plastic substrate and plots for OTFT; (c) transfer characteristic (I_{DS}–V_{GS}), when $V_{DS} = -2$ V, and (d) output characteristic (I_{DS}–V_{DS}), where V_{GS} ranges from 0 to −15 V at −3 V step.

voltage (I_{DS}–V_{GS}) transfer curve of Fig. 5c, the OTFT with the $AdUr_4$ dielectric layer displayed an average field mobility of 0.15 $cm^2\ V^{-1}\ s^{-1}$ at −45 V, threshold voltages (V_{th}) of −3 V, an on/off current ratio of 2.18 × 10^4. Regioregular, P3HT is a material of choice for research OTFTs because of its high field effect mobility, stability, and solution processability. The orientation of P3HT molecular chains *i.e.* parallel (face-on structure) or perpendicular (edge-on structure) to the insulator substrate is an important phenomenon which need to be explored for the optimum performance of OTFTs. This phenomenon is much dependent on the chemical nature of the gate insulator material as it is the penultimate layer on which semiconducting layer is spin-casted. To study the structural ordering of spin coated films of P3HT on the insulator surface ($AdUr_4$), we used synchrotron grazing-incidence X-ray diffraction (GI-XRD). The grazing incidence angle of 0.18° was employed and in order to isolate the scattering data from the P3HT polymer film only, the scan from a bare insulator substrate was used to remove background.[42] The GI-XRD result is shown in Fig. 6a which demonstrates that the nanocrystalline regioregular P3HT molecular domains has mainly preferred to crystallize in edge-on orientation over the $AdUr_4$ gate insulator

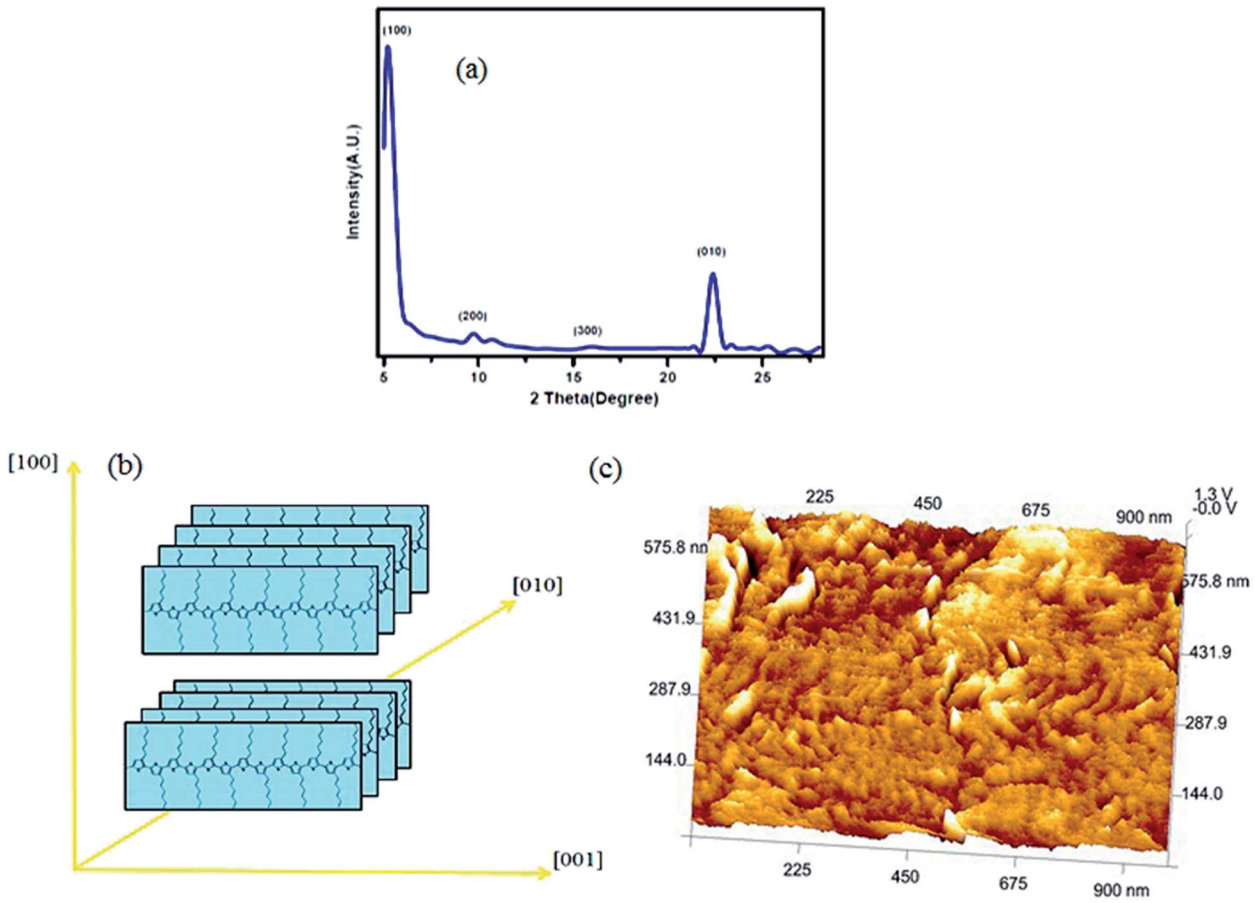

Fig. 6 (a) Out of plane grazing-incidence angle X-ray diffraction intensities as a function of the scattering angle 2θ for regioregular P3HT thin films crystallized against insulator material $AdUr_4$ on silicon wafer. (b) The insets show schematically the crystallography of the P3HT nanocrystallites with respect to the insulator material, $AdUr_4$ (c) tapping phase mode AFM image of a regioregular P3HT film against the $AdUr_4$ insulator on flexible PI substrates.

as compared to their possible face-on orientation. These two different chain orientations of nanocrystalline regioregular P3HT domains with respect to the $AdUr_4$ STF are evident from the different intensity distribution of the (100) reflections due to the lamellar layer structure (16.4 Å) and the (010) reflections due to interchain stacking (3.8 Å) through out-of-plane and in-plane geometric mode.[12a,b] The intense (100) reflections in the XRD spectra with respect to the (010) reflections shows that on $AdUr_4$ STF the P3HT molecular chain domains has preferred to crystallize in edge on orientations, as shown in Fig. 6b. The GI-XRD has revealed this type of nanocrystalline structural order that has prevailed throughout the P3HT film, while the AFM observations was further done to provide images of the top surface. Fig. 6c, shows AFM topographic image of regioregular P3HT thin films on insulator substrate ($AdUr_4$). The wormlike morphology of P3HT molecular chains in AFM image, has arisen because of their perpendicular orientations over insulator substrate ($AdUr_4$).[12a] This edge on orientation of P3HT chains has led to their enhanced π–π stacking in the direction of charge transfer in OTFT.

The presence of uracil moiety at the 1,3,5,7 position of the adamantane, in $AdUr_4$ STF has played an important role in the appearance of edge on orientation of P3HT molecular chain domains. The $AdUr_4$ molecules first undergoes adsorption on gold coated PI plastic substrate and then form $AdUr_4$ STF through U···U intermolecular hydrogen bonds. The FTIR spectra of $AdUr_4$ STF in Fig. 4b, shows that, their exist two type of –NH protons in uracil substructure. The one which are involved in intermolecular hydrogen bonding shows their characteristic peak at 3188 cm^{-1} while the other, free –NH protons which are not involved in intermolecular hydrogen bonding appears at 3475 cm^{-1}. The free polar –NH protons have undergone π–H interaction (attractive) with thienyl backbone of the regioregular P3HT molecular chains. However, the lone pair of electrons on other type of (–NH)˙˙ protons in $AdUr_4$ STF were involved in repulsion force with the π-electron cloud of the P3HT molecular chains. Therefore, the P3HT molecular chain domains experiences two opposite force of interactions, over the $AdUr_4$ gate insulator thin film. These two counter forces *i.e.* force of attraction and repulsion makes the regioregular P3HT molecular chains to pack into the edge-on orientation, *i.e.* perpendicular to the insulator substrate.[12a,b]

Fig. 7 shows this whole mechanism of formation of edge-on orientation of P3HT molecular chains over $AdUr_4$ STF dielectric layer. Further, the adamantane is a rigid tetrahedral molecule[21] hence during molecular packing of the $AdUr_4$ molecules in the form of STF there may exist some voids in them. In these voids the hexane chains on the backbone of P3HT stucks, which further helps the regioregular P3HT molecular chains to crystallize in edge-on orientations. These all factors has led to the success of our P3HT based OTFT device as fabricated with new gate insulator layer material $AdUr_4$.

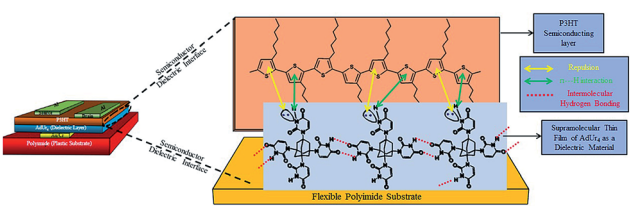

Fig. 7 Bottom gate flexible thin film transistor configuration with schematic representation of P3HT polymer chains undergoing edge-on orientation against the $AdUr_4$ insulator surface.

4. Conclusion

The recent advances in flexible OTFTs have highlighted the use of low cost technology and materials to replace the most commonly used semiconductor and dielectric materials. We have successfully synthesized new dielectric materials $AdCl_4$, $AdBr_4$, AdI_4 and $AdUr_4$ through easy to follow synthesis process. Their potential to act as a dielectric material was analysed by fabrication of MIM devices respectively from them. The comparisons of *I–V* characteristics study of these respective MIM devices have showed that $AdUr_4$ is a better insulator material for plastic electronics. The ability of $AdUr_4$ molecules to undergo supramolecular thin film formation through intermolecular hydrogen bonding has been successfully explored here. Its use as a gate electrode in electronic devices, through fabrication of a new and fully flexible P3HT, a p-type OTFT on the flexible PI plastic substrate has also been demonstrated in this work. This P3HT based OTFT device incorporated with $AdUr_4$ as a gate electrode showed good on/off current ratio (2.18×10^4) and high charge mobility (0.15 $cm^2\ V^{-1}\ s^{-1}$). The detailed semiconductor–dielectric interface study, lead us to conclude that the P3HT molecular chain domains has undergone edge-on crystallization (perpendicular to the insulator substrate), *i.e.* the charge transport direction in OTFTs. This study has explored a new efficient pathway for development of flexible OTFTs to their full potential on commercial scale, by exploiting the self-assembling ability of small molecules into thin films as a dielectric material in them.

Acknowledgements

The authors are grateful to the National Device Laboratories for their support in the device fabrication, the National Science Council of Taiwan for financially supporting this research under the contract NSC 101-2113-M-009-MY3.

Notes and references

1 (*a*) H. Sirringhaus, *Adv. Mater.*, 2005, **17**, 2411; (*b*) R. A. Street, *Adv. Mater.*, 2009, **21**, 2007; (*c*) G. Malliaras and R. H. Friend, *Phys. Today*, 2005, **58**, 53; (*d*) S. J. Kim and J. S. Lee, *Nano Lett.*, 2010, **10**, 2884.

2 (*a*) P. M. Beaujuge and J. M. Frechet, *J. Am. Chem. Soc.*, 2011, **133**, 20009; (*b*) C. Wang, H. Dong, W. Hu, Y. Liu and D. Zhu, *Chem. Rev.*, 2012, **112**, 2208; (*c*) V. C. Sundar, J. Zaumseil, V. Podzorov, E. Menard, R. L. Willett, T. Someya, M. E. Gershenson and J. A. Rogers, *Science*, 2004, **303**, 1644; (*d*) M. Kaltenbrunner, T. Sekitani, J. Reeder, T. Yokota, K. Kuribara, T. Tokuhara, M. Drack,

R. Schwodiauer, I. Graz, S. Bauer-Gogonea, S. Bauer and T. Someya, *Nature*, 2013, **499**, 458.

3 (*a*) E. J. Meijer, D. M. De Leeuw, S. Setayesh, E. Van Veenendaal, B. H. Huisman, P. W. M. Blom, J. C. Hummelen, U. Scherf and T. M. Klapwijk, *Nat. Mater.*, 2003, **2**, 678; (*b*) H. U. Khan, M. E. Roberts, W. Knoll and Z. N. Bao, *Chem. Mater.*, 2011, **23**, 1946; (*c*) T. Sekitani, U. Zschieschang, H. Klauk and T. Someya, *Nat. Mater.*, 2010, **9**, 1015; (*d*) H. Sirringhaus, T. Kawase, R. H. Friend, T. Shimoda, M. Inbasekaran, W. Wu and P. E. Woo, *Science*, 2000, **290**, 2123.

4 (*a*) K. Cherenack and L. van Pieterson, *J. Appl. Phys.*, 2012, **112**, 091301; (*b*) M. S. White, M. Kaltenbrunner, E. D. Głowacki, K. Gutnichenko, G. Kettlgruber, I. Graz, S. Aazou, C. Ulbricht, D. A. M. Egbe, M. C. Miron, Z. Major, M. C. Scharber, T. Sekitani, T. Someya, S. Bauer and N. S. Sariciftci, *Nat. Photonics*, 2013, **7**, 811; (*c*) X. H. Zhang Jr, W. J. Potscavage, S. K. Choi and B. Kippelen, *Appl. Phys. Lett.*, 2009, **94**, 043312; (*d*) R. Rotzoll, S. Mohapatra, V. Olariu, R. Wenz, M. Grigas and K. Dimmler, *Appl. Phys. Lett.*, 2006, **88**, 123502.

5 (*a*) M. L. Chabinyc, F. Endicott, B. D. Vogt, D. M. DeLongchamp, E. K. Lin, Y. Wu, P. Liu and B. S. Ong, *Appl. Phys. Lett.*, 2006, **88**, 113514; (*b*) H. Sirringhaus, *Adv. Mater.*, 2009, **21**, 3859; (*c*) A. Facchetti, *Chem. Mater.*, 2011, **23**, 733.

6 (*a*) X. Zhang, H. Bronstein, A. J. Kronemeijer, J. Smith, Y. Kim, R. J. Kline, L. J. Richter, T. D. Anthopoulos, H. Sirringhaus, K. Song, M. Heeney, W. Zhang, I. McCulloch and D. M. DeLongchamp, *Nat. Commun.*, 2013, **4**, 2238; (*b*) C. Gu, W. Hu, J. Yao and H. Fu, *Chem. Mater.*, 2013, **25**, 2178; (*c*) R. P. Ortiz, A. Facchetti and T. J. Marks, *Chem. Rev.*, 2010, **110**, 205.

7 (*a*) K.-J. Baeg, M. Caironi and Y.-Y. Noh, *Adv. Mater.*, 2013, **25**, 4210; (*b*) J. Lee, J. Han, A.-R. Kim, Y. Kim, J. H. Oh and C. Yang, *J. Am. Chem. Soc.*, 2012, **134**, 20713; (*c*) J. Li, Y. Zhao, H. S. Tan, Y. Guo, C.-A. Di, G. Yu, Y. Liu, M. Lin, S. H. Lim, Y. Zhou, H. Su and B. S. Ong, *Sci. Rep.*, 2012, **2**, 754.

8 I. McCulloch, *Adv. Mater.*, 2013, **25**, 1811.

9 S. M. Sze, *Semiconductor Devices: Physics and Technology*, Wiley, New York, 2nd edn, 1981.

10 (*a*) S. Wu, M. Shao, Q. Burlingame, X. Chen, M. Lin, K. Xiao and Q. M. Zhang, *Appl. Phys. Lett.*, 2013, **102**, 013301; (*b*) G. Lucovsky and V. Misra, *Encyclopedia of Materials: Science and Technology*, 2001, 2nd edn, p. 2070; (*c*) C. Liu, Y. Xu, Y. Li, W. Scheideler and T. Minari, *J. Phys. Chem. C*, 2013, **117**, 12337.

11 (*a*) A. Facchetti, M.-H. Yoon and T. J. Marks, *Adv. Mater.*, 2005, **17**, 1705; (*b*) D. Natali and M. Caironi, *Adv. Mater.*, 2012, **24**, 1357; (*c*) S. Alexander, A. S. Eggeman, S. Illig, A. Troisi, H. Sirringhaus and P. A. Midgley, *Nat. Mater.*, 2013, **12**, 1045–1049.

12 (*a*) D. H. Kim, Y. D. Park, Y. Jang, H. Yang, Y. H. Kim, J. I. Han, D. G. Moon, S. Park, T. Chang, C. Chang, M. Joo, C. Y. Ryu and K. Cho, *Adv. Funct. Mater.*, 2005, **15**, 17; (*b*) H. Yang, T. J. Shin, L. Yang, K. Cho, C. Y. Ryu and Z. Bao, *Adv. Funct. Mater.*, 2005, **15**, 671; (*c*) X. Xu, B. Liu, Y. Zou, Y. Guo, L. Li and Y. Liu, *Adv. Funct. Mater.*, 2012, **22**, 4139; (*d*) H. Ma, H.-L. Yip, F. Huang and A. K.-Y. Jen, *Adv. Funct. Mater.*, 2010, **20**, 1371.

13 C.-H. Wang, C.-Y. Hsieh and J.-C. Hwang, *Adv. Mater.*, 2011, **23**, 1630.

14 (*a*) N. B. Ukah, J. Granstrom, R. R. S. Gari, G. M. King and S. Guha, *Appl. Phys. Lett.*, 2011, **99**, 243302; (*b*) J. Li, D. Liu, Q. Miaob and F. Feng Yan, *J. Mater. Chem.*, 2012, **22**, 15998; (*c*) M. Caironi, E. Gili and H. Sirringhaus, Ink-Jet Printing of Downscaled Organic Electronic Devices, in *Organic Electronics II: More Materials and Applications*, ed. H. Klauk, Wiley-VCH Verlag GmbH &Co. KGaA, Weinheim, Germany. 2012, ch. 9, DOI: 10.1002/9783527640218; (*d*) J. S. Meena, M.-C. Chu, Y.-C. Chang, C.-S. Wu, C.-C. Cheng, F.-C. Chang and F.-H. Ko, *ACS Appl. Mater. Interfaces*, 2012, **4**, 3261.

15 (*a*) Y. Yun, C. Pearson and M. C. Petty, *J. Appl. Phys.*, 2009, **105**, 034508; (*b*) H. Yan, Z. Chen, Y. Zheng, C. Newman, J. R. Quinn, F. Dötz, M. Kastler and A. Facchetti, *Nature*, 2009, **457**, 679; (*c*) F. D. Angelis, S. Cipolloni, L. Mariucci and G. Ortunato, *Appl. Phys. Lett.*, 2005, **86**, 203505; (*d*) T.-W. Lee, Y. H. Byun, B. W. Koo, I.-N. Kang, Y.-Y. Lyu, C. H. Lee, L. S. Pu and S. Y. Lee, *Adv. Mater.*, 2005, **17**, 2180.

16 (*a*) J. Park, S. Y. Park, S. O. Shim, H. Kang and H. H. Lee, *Appl. Phys. Lett.*, 2004, **85**, 3283; (*b*) S. H. Lim, J. Kim, S.-G. Lee and Y. S. Kim, *Chem. Commun.*, 2010, **46**, 3961.

17 (*a*) Y. Fujisaki, Y. Nakajima, D. Kumaki, T. Yamamoto, S. Tokito, T. Kono, J. Nishida and Y. Yamashita, *Appl. Phys. Lett.*, 2010, **97**, 133303; (*b*) W. Xu, C. Guo and S. W. Rhee, *J. Mater. Chem.*, 2012, **22**, 6597; (*c*) T.-W. Lee, J. H. Shin, I.-N. Kang and S. Y. Lee, *Adv. Mater.*, 2007, **19**, 2702.

18 (*a*) H. Klauk, M. Halik, U. Zschieschang, G. Schmid, W. Radlik and W. J. Weber, *J. Appl. Phys.*, 2002, **92**, 5259; (*b*) S. M. Pyo, M. Y. Lee, J. Jeon, J. H. Lee, M. H. Yi and J. S. Kim, *Adv. Funct. Mater.*, 2005, **15**, 619; (*c*) A. A. Virkar, S. Mannsfeld, Z. Bao and N. Stingelin, *Adv. Mater.*, 2010, **22**, 3857.

19 (*a*) S. F. Adams and L. H. Caveny, *AIP Conf. Proc.*, 1992, **246**, 643; (*b*) W. A. de Heer, J.-M. Bonard, K. Fauth, A. Châtelain, D. Ugarte and L. Forró, *Adv. Mater.*, 1997, **9**, 87.

20 (*a*) S. Landa and V. Machacek, *Collect. Czech. Chem. Commun.*, 1933, **5**, 1; (*b*) G. Guangli Wang, S. Shengbao Shi, P. Wang and T.-G. Wang, *Fuel*, 2013, **107**, 706; (*c*) A. T. Balaban, *J. Chem. Inf. Model.*, 2012, **52**, 2856; (*d*) B. J. Mair, M. Shamaiengar, N. C. Krouskop and F. D. Rossini, *Anal. Chem.*, 1959, **31**, 2082; (*e*) L. J. Mathias, V. R. Reichert and A. V. G. Muirl, *Chem. Mater.*, 1993, **5**, 4.

21 (*a*) K. Morita, T. Hashimoto, M. Urushisaki and T. Sakaguchi, *J. Polym. Sci., Part A: Polym. Chem.*, 2013, **51**, 2445; (*b*) A.-Y. Jee and M. Lee, *Carbon*, 2009, **47**, 2546; (*c*) E. M. Maya, I. García-Yoldi, A. E. Lozano, J. G. de la Campa and J. de Abajo, *Macromolecules*, 2011, **44**, 2780; (*d*) S. Zheng, J. Shi and R. Mateu, *Chem. Mater.*, 2000, **12**, 1814; (*e*) L. J. Mathias, J. J. Jensen, V. T. Reichert, C. M. Lewis and G. L. Tullos, *ACS Symp. Ser.*, 1996, **624**, 197.

22 H. Schwertfeger, A. A. Fokin and P. R. Schreiner, *Angew. Chem., Int. Ed.*, 2008, **47**, 1022.

23 (*a*) R. C. Fort and P. R. Schleyer, *Chem. Rev.*, 1964, **64**, 277; (*b*) J. E. Dahl, S. G. Liu and R. M. K. Carlson, *Science*, 2003, **299**, 96; (*c*) A. P. Marchand, *Science*, 2002, **299**, 52.

24 (*a*) S. D. Banister, S. M. Wilkinson, M. Longworth, J. Stuart, N. Apetz, K. English, L. Brooker, C. Goebe, D. E. Hibbs, M. Glass, M. Connor, L. S. McGregor and M. Kassiou, *ACS Chem. Neurosci.*, 2013, **4**, 1081; (*b*) L. Wanka, I. Khalid and P. R. Schreiner, *Chem. Rev.*, 2013, **113**, 3516; (*c*) J. Zhang, Z. Zhu, Y. Feng, H. Ishiwata, Y. Miyata, R. Kitaura, J. E. P. Dahl, R. M. K. Carlson, N. A. Fokina, P. R. Schreiner, D. Tománek and H. Shinohara, *Angew. Chem., Int. Ed.*, 2013, **52**, 3717; (*d*) P.-L. E. Chu, L.-Y. Wang, S. Khatua, A. B. Kolomeisky, S. Link and J. M. Tour, *ACS Nano*, 2013, **7**, 35.

25 (*a*) T. Strunskus, M. Grunze, G. Kochendoerfer and C. Wöll, *Langmuir*, 1996, **12**, 2712; (*b*) E. Lindner and R. P. Buck, *Anal. Chem.*, 2000, **72**, 336A.

26 (*a*) P. R. Schreiner, N. A. Fokina, B. A. Tkachenko, H. Hausmann, M. Serafin, J. E. P. Dahl, S. Liu, R. M. K. Carlson and A. A. Fokin, *J. Org. Chem.*, 2006, **71**, 6709; (*b*) M. Vörös, T. Demjén, T. Szilvási and A. Gali, *Phys. Rev. Lett.*, 2012, **108**, 267401; (*c*) A. Patzer, M. Schütz, T. Möller and O. Dopfer, *Angew. Chem.*, 2012, **124**, 5009.

27 G. S. Lee, J. N. Bashara, G. Sabih, A. Oganesyan, G. Godjoian, H. M. Duong, E. R. Marinez and C. G. Gutiérrez, *Org. Lett.*, 2004, **6**, 1705.

28 (*a*) Z. Ding, R. Xing, Y. Sun, L. Zheng, X. Wang, J. Ding, L. Wanga and Y. Han, *RSC Adv.*, 2013, **3**, 8037; (*b*) J.-N. Tisserant, G. Wicht, O. F. Göbel, E. Bocek, G.-L. Bona, T. Geiger, R. Hany, R. Mezzenga, S. Partel, P. Schmid, W. B. Schweizer and J. Heier, *ACS Nano*, 2013, **7**, 5506; (*c*) A. Datar, R. Oitker and L. Zang, Surface-Assisted One Dimensional Self-Assembly of a Perylene Based Semiconductor Molecule, *Chem. Commun.*, 2006, 1649; (*d*) Y. Su, J. Liu, L. Zheng, Z. Ding and Y. Han, *RSC Adv.*, 2012, **2**, 5779.

29 (*a*) N. K. Nath, B. K. Saha and A. I. Nangia, *New J. Chem.*, 2008, **32**, 1693; (*b*) P. V. Gushchin, M. L. Kuznetsov, M. Haukka and V. Y. Kukushkin, *J. Phys. Chem. A*, 2013, **117**, 2827; (*c*) F. Zordan, L. Brammer and P. Sherwood, *J. Am. Chem. Soc.*, 2005, **127**, 5979; (*d*) R. Gutzler, C. Fu, A. Dadvand, Y. Hua, J. M. MacLeod, F. Rosei and D. F. Perepichka, *Nanoscale.*, 2012, **4**, 5965.

30 V. R. Pedireddi, D. S. Reddy, B. S. Goud, D. C. Craig, A. D. Rae and G. R. Desiraju, *J. Chem. Soc., Perkin Trans. 2*, 1994, **2**, 2353.

31 (*a*) M. V. Vener, A. V. Shishkina, A. A. Rykounov and V. G. Tsirelson, *J. Phys. Chem. A*, 2013, **117**, 8459; (*b*) R. S. Rowland and R. Taylor, *J. Phys. Chem. A*, 1996, **100**, 7384; (*c*) Y. V. Zefirov and A. V. Churakov, *Russ. J. Inorg. Chem.*, 2000, **45**, 1880.

32 (*a*) S. Irrera, A. Roldan, G. Portalone and N. H. De Leeuw, *J. Phys. Chem. C*, 2013, **117**, 3949; (*b*) S. Irrera and N. H. De Leeuw, *Proc. R. Soc. A*, 2011, **467**, 1959; (*c*) D. M. A. Smith, J. Smets and L. J. Adamowicz, *J. Phys. Chem. A*, 1999, **103**, 5784.

33 (*a*) S. E. Fritz, T. W. Kelley and C. D. Frisbie, *J. Phys. Chem. B*, 2005, **109**, 10574; (*b*) H. Yang, C. Yang, S. H. Kim, M. Jang and C. E. Park, *ACS Appl. Mater. Interfaces*, 2010, **2**, 391.

34 M. R. Scholfield, C. M. V. Zanden, M. Carter and P. S. Ho, *Protein Sci.*, 2013, **22**, 139.

35 J. C. Slater, *J. Chem. Phys.*, 1964, **41**, 3199.

36 (*a*) Y.-M. Zhang, C. Cao, Y. Y. Lu, Q. S. Zhang and T. B. Wei, *Acta Crystallogr., Sect. E: Struct. Rep. Online*, 2011, **67**, o286; (*b*) P. R. Schreiner, L. V. Chernish, P. A. Gunchenko, E. Y. Tikhonchuk, H. H. Hausmann, M. Serafin, S. Schlecht, J. E. P. Dahl, R. M. K. Carlson and A. A. Fokin, *Nature*, 2011, **477**, 308; (*c*) W. Guo, E. Galoppini, R. Gilardi, G. I. Rydja and Y.-H. Chen, *Cryst. Growth Des.*, 2001, **1**, 231; (*d*) M. F. Roll, J. W. Kampf and R. M. Laine, *Cryst. Growth Des.*, 2011, **11**, 4360–4367.

37 (*a*) J. D. Dunitz and A. Gavezzotti, *Chem. Soc. Rev.*, 2009, **38**, 2622; (*b*) J. S. Ovens, K. N. Truonga and D. B. Leznoff, *Dalton Trans.*, 2012, **41**, 1345; (*c*) G. Song, L. Zhang, C. He, D.-C. Fang, P. G. Whitten and H. Wang, *Macromolecules*, 2013, **46**, 7423.

38 M. Kawamura, Y. Nakahara, M. Ohse, M. Kumei, K. Uno, H. Sakamoto, K. Kimura and I. Tanaka, *Appl. Phys. Lett.*, 2012, **101**, 053311.

39 (*a*) P. Politzer and J. S. Murray, *ChemPhysChem*, 2013, **14**, 278; (*b*) H. Wang, X. R. Zhao and W. J. Jin, *Phys. Chem. Chem. Phys.*, 2013, **15**, 4320; (*c*) P. Metrangolo, H. Neukirch, T. Pilati and G. Resnati, *Acc. Chem. Res.*, 2005, **38**, 386.

40 (*a*) T. Dretschkow, A. S. Dakkouri and T. Wandlowski, *Langmuir*, 1997, **13**, 2843; (*b*) S. Irrera, G. Portalone and N. De Leeuw, *Surf. Sci.*, 2013, **614**, 20; (*c*) S. Irrera, A. Roldan, G. Portalone and N. De Leeuw, *J. Phys. Chem. C*, 2013, **117**, 3949; (*d*) A. C. Papageorgiou, S. Fischer, J. Reichert, K. Diller, F. Blobner, F. Klappenberger, F. Allegretti, A. P. Seitsonen and J. V. Barth, *ACS Nano*, 2012, **6**, 2477; (*e*) H. B. de Aguiar, F. G. C. Cunha, F. C. Nart and P. B. Miranda, *J. Phys. Chem. C*, 2010, **114**, 6663.

41 (*a*) M. S. Masouda, A. A. Ibrahim, E. A. Khalil and A. El-Marghany, *Spectrochim. Acta, Part A*, 2007, **67**, 662; (*b*) S. Sivakova and J. S. Rowan, *Chem. Soc. Rev.*, 2005, **34**, 9; (*c*) C. C. Cheng, Y.-L. Chu, P.-H. Huang, Y.-C. Yen, C.-W. Chu, A. C.-M. Yang, F.-H. Ko, J.-K. Chen and F.-C. Chang, *J. Mater. Chem.*, 2012, **22**, 18127; (*d*) E. M. B. Janke and K. Weisz, *J. Phys. Chem. B*, 2013, **117**, 4853.

42 (*a*) J. Kim, E. Ryba and J. Bai, *Polymer*, 2003, **44**, 6663; (*b*) M. Birkholz, *Thin Film Analysis by X-Ray Scattering*, Wiley-VCH, Weinheim, Germany, 2006, p. 155.

